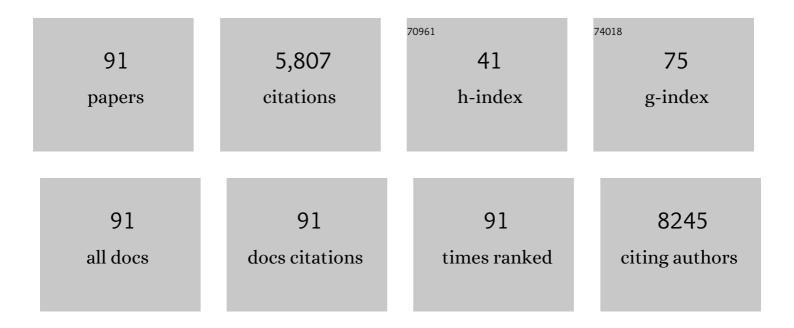
Baorui Xia

List of Publications by Year in descending order

Source: https://exaly.com/author-pdf/3296128/publications.pdf Version: 2024-02-01



ΒλΟΡΙΙΙ ΧΙΛ

#	Article	IF	CITATIONS
1	Atomic-level coupled spinel@perovskite dual-phase oxides toward enhanced performance in Zn–air batteries. Journal of Materials Chemistry A, 2022, 10, 1506-1513.	5.2	28
2	Significant Change of Metal Cations in Geometric Sites by Magneticâ€Field Annealing FeCo ₂ O ₄ for Enhanced Oxygen Catalytic Activity. Small, 2022, 18, e2104248.	5.2	21
3	High efficiency electrocatalyst of LaNiO3@LaCoO3 nanoparticles on oxygen-evolution reaction. FlatChem, 2022, , 100371.	2.8	0
4	Fluorination activates the basal plane HER activity of ReS ₂ : a combined experimental and theoretical study. Journal of Materials Chemistry A, 2021, 9, 14451-14458.	5.2	21
5	Optimized Conductivity and Spin States in N-Doped LaCoO ₃ for Oxygen Electrocatalysis. ACS Applied Materials & Interfaces, 2021, 13, 2447-2454.	4.0	34
6	Insights into Bimetallic Oxide Synergy during Carbon Dioxide Hydrogenation to Methanol and Dimethyl Ether over GaZrO _{<i>x</i>} Oxide Catalysts. ACS Catalysis, 2021, 11, 4704-4711.	5.5	60
7	Cr cation-anchored carbon nanosheets: synthesis, paramagnetism and ferromagnetism. Nanotechnology, 2021, 32, 335706.	1.3	2
8	Surface-Electronic-Structure Reconstruction of Perovskite via Double-Cation Gradient Etching for Superior Water Oxidation. Nano Letters, 2021, 21, 8166-8174.	4.5	29
9	Ferromagnetism of two-dimensional transition metal chalcogenides: both theoretical and experimental investigations. Nanoscale, 2021, 13, 12772-12787.	2.8	12
10	Hydrogen-etched CoS ₂ to produce a Co ₉ S ₈ @CoS ₂ heterostructure electrocatalyst for highly efficient oxygen evolution reaction. RSC Advances, 2021, 11, 30448-30454.	1.7	12
11	Tunable ferromagnetic ordering in phosphorus adsorbed ReS2 nanosheets. Nanotechnology, 2021, 32, 075701.	1.3	2
12	Energy-level engineered hollow N-doped NiS1.03 for Zn–Air batteries. Energy Storage Materials, 2020, 25, 202-209.	9.5	62
13	Engineering Lower Coordination Atoms onto NiO/Co ₃ O ₄ Heterointerfaces for Boosting Oxygen Evolution Reactions. ACS Catalysis, 2020, 10, 12376-12384.	5.5	223
14	Engineering the Nucleophilic Active Oxygen Species in CuTiO _{<i>x</i>} for Efficient Low-Temperature Propene Combustion. Environmental Science & Technology, 2020, 54, 15476-15488.	4.6	48
15	High efficiency electrocatalyst of LaCr0.5Fe0.5O3 nanoparticles on oxygen-evolution reaction. Scientific Reports, 2020, 10, 13395.	1.6	17
16	Efficient electrocatalyst of α-Fe ₂ O ₃ nanorings for oxygen evolution reaction in acidic conditions. RSC Advances, 2020, 10, 29077-29081.	1.7	6
17	Giant magnetoelectric coupling observed at high frequency in NiFe ₂ O ₄ –BaTiO ₃ particulate composite. RSC Advances, 2020, 10, 27242-27248.	1.7	10
18	Enhanced thermal stability of lead-free (1-x)Ba(Zr0.2Ti0.8)O3-x(Ba0.7Ca0.3)TiO3 ferroelectric ceramics. Journal of Materials Science, 2020, 55, 16890-16899.	1.7	6

Baorui Xia

#	Article	IF	CITATIONS
19	A Co ₃ O ₄ /MnCO ₃ heterojunction on three-dimensional nickel foam for an enhanced oxygen evolution reaction. CrystEngComm, 2020, 22, 3984-3990.	1.3	7
20	Aliovalent fluorine doping and anodization-induced amorphization enable bifunctional catalysts for efficient water splitting. Journal of Materials Chemistry A, 2020, 8, 10831-10838.	5.2	31
21	Nitrogen-doped RuS ₂ nanoparticles containing <i>in situ</i> reduced Ru as an efficient electrocatalyst for hydrogen evolution. RSC Advances, 2020, 10, 17862-17868.	1.7	6
22	Bifunctional Oxygen Electrocatalyst of Mesoporous Ni/NiO Nanosheets for Flexible Rechargeable Zn–Air Batteries. Nano-Micro Letters, 2020, 12, 68.	14.4	103
23	Interfacial Engineering of NiO/NiCo ₂ O ₄ Porous Nanofibers as Efficient Bifunctional Catalysts for Rechargeable Zinc–Air Batteries. ACS Applied Materials & Interfaces, 2020, 12, 21661-21669.	4.0	80
24	Realization of "single-atom ferromagnetism―in graphene by Cu–N4 moieties anchoring. Applied Physics Letters, 2020, 116, .	1.5	9
25	Tunable Fe3O4 Nanorods for Enhanced Magnetic Hyperthermia Performance. Scientific Reports, 2020, 10, 8331.	1.6	28
26	On-chip scalable mode-selective converter based on asymmetrical micro-racetrack resonators. Nanophotonics, 2020, 9, 1447-1455.	2.9	3
27	Ferromagnetic Cu ₃ N Nanoparticles Demonstrated by X-ray Magnetic Circular Dichroism (XMCD) and the Density Functional Theory (DFT) Calculations. Journal of Nanoelectronics and Optoelectronics, 2020, 15, 1494-1501.	0.1	2
28	Bifunctional Electrocatalytic Activity of Nitrogen-Doped NiO Nanosheets for Rechargeable Zinc–Air Batteries. ACS Applied Materials & Interfaces, 2019, 11, 30865-30871.	4.0	41
29	Bifunctional catalysts of CoNi nanoparticle-embedded nitrogen-doped carbon nanotubes for rechargeable Zn–air batteries. Nanotechnology, 2019, 30, 435701.	1.3	20
30	Expediting in-Situ Electrochemical Activation of Two-Dimensional Metal–Organic Frameworks for Enhanced OER Intrinsic Activity by Iron Incorporation. ACS Catalysis, 2019, 9, 7356-7364.	5.5	215
31	A large enhancement of magnetism in zigzag Janus MoSSe nanoribbons: First-principles calculations. Europhysics Letters, 2019, 127, 46003.	0.7	4
32	N ⁺ -ion irradiation engineering towards the efficient oxygen evolution reaction on NiO nanosheet arrays. Journal of Materials Chemistry A, 2019, 7, 4729-4733.	5.2	48
33	Electronic structure modulation of NiS ₂ by transition metal doping for accelerating the hydrogen evolution reaction. Journal of Materials Chemistry A, 2019, 7, 4971-4976.	5.2	93
34	Cu and Co nanoparticle-Co-decorated N-doped graphene nanosheets: a high efficiency bifunctional electrocatalyst for rechargeable Zn–air batteries. Journal of Materials Chemistry A, 2019, 7, 12851-12858.	5.2	50
35	Bifunctional porous Co-doped NiO nanoflowers electrocatalysts for rechargeable zinc-air batteries. Applied Catalysis B: Environmental, 2019, 250, 71-77.	10.8	98
36	Phosphorus dual-site driven CoS ₂ @S, N co-doped porous carbon nanosheets for flexible quasi-solid-state supercapacitors. Journal of Materials Chemistry A, 2019, 7, 26618-26630.	5.2	82

Baorui Xia

#	Article	IF	CITATIONS
37	High-Magnetization Tetragonal Ferrite-Based Films Induced by Carbon and Oxygen Vacancy Pairs. ACS Applied Materials & Interfaces, 2019, 11, 1049-1056.	4.0	5
38	Bimetallic Nickel Cobalt Sulfide as Efficient Electrocatalyst for Zn–Air Battery and Water Splitting. Nano-Micro Letters, 2019, 11, 2.	14.4	179
39	Dualâ€Native Vacancy Activated Basal Plane and Conductivity of MoSe ₂ with Highâ€Efficiency Hydrogen Evolution Reaction. Small, 2018, 14, e1704150.	5.2	114
40	Accelerated Hydrogen Evolution Reaction in CoS ₂ by Transition-Metal Doping. ACS Energy Letters, 2018, 3, 779-786.	8.8	231
41	Selfâ€Powered Waterâ€Splitting Devices by Core–Shell NiFe@Nâ€Graphiteâ€Based Zn–Air Batteries. Advanc Functional Materials, 2018, 28, 1706928.	ed. ₈	155
42	Activation of the MoSe ₂ basal plane and Se-edge by B doping for enhanced hydrogen evolution. Journal of Materials Chemistry A, 2018, 6, 510-515.	5.2	110
43	Re doping induced 2H-1T phase transformation and ferromagnetism in MoS2 nanosheets. Applied Physics Letters, 2018, 113, .	1.5	45
44	Transition-metal-doped NiSe2 nanosheets towards efficient hydrogen evolution reactions. Nano Research, 2018, 11, 6051-6061.	5.8	72
45	A low crystallinity oxygen-vacancy-rich Co ₃ O ₄ cathode for high-performance flexible asymmetric supercapacitors. Journal of Materials Chemistry A, 2018, 6, 16094-16100.	5.2	182
46	Ar ²⁺ Beam Irradiation-Induced Multivancancies in MoSe ₂ Nanosheet for Enhanced Electrochemical Hydrogen Evolution. ACS Energy Letters, 2018, 3, 2167-2172.	8.8	73
47	Efficient visible light-induced degradation of rhodamine B by W(NxS1â^'x)2 nanoflowers. Scientific Reports, 2017, 7, 40784.	1.6	10
48	Activating and Optimizing Activity of CoS ₂ for Hydrogen Evolution Reaction through the Synergic Effect of N Dopants and S Vacancies. ACS Energy Letters, 2017, 2, 1022-1028.	8.8	229
49	Phase-transfer induced room temperature ferromagnetic behavior in 1T@2H-MoSe2 nanosheets. Scientific Reports, 2017, 7, 45307.	1.6	23
50	Dualâ€Functional N Dopants in Edges and Basal Plane of MoS ₂ Nanosheets Toward Efficient and Durable Hydrogen Evolution. Advanced Energy Materials, 2017, 7, 1602086.	10.2	286
51	Copper dopants improved the hydrogen evolution activity of earth-abundant cobalt pyrite catalysts by activating the electrocatalytically inert sulfur sites. Journal of Materials Chemistry A, 2017, 5, 17601-17608.	5.2	61
52	Anion vacancy-mediated ferromagnetism in atomic-thick Ni3N nanosheets. Applied Physics Letters, 2017, 111, .	1.5	11
53	Metallic Ni ₃ N nanosheets with exposed active surface sites for efficient hydrogen evolution. Journal of Materials Chemistry A, 2016, 4, 17363-17369.	5.2	233
54	Atomically Thin B doped g-C3N4 Nanosheets: High-Temperature Ferromagnetism and calculated Half-Metallicity. Scientific Reports, 2016, 6, 35768.	1.6	74

BAORUI XIA

#	Article	IF	CITATIONS
55	N-doped WS ₂ nanosheets: a high-performance electrocatalyst for the hydrogen evolution reaction. Journal of Materials Chemistry A, 2016, 4, 11234-11238.	5.2	147
56	Cu vacancies modulated the room temperature ferromagnetism in Cu ₂ O/Cu nanoparticle composites. CrystEngComm, 2015, 17, 2118-2122.	1.3	9
57	Zigzag-edge related ferromagnetism in MoSe ₂ nanoflakes. Physical Chemistry Chemical Physics, 2015, 17, 32505-32510.	1.3	26
58	Manifestation of high-temperature ferromagnetism in fluorinated graphitic carbon nitride nanosheets. Journal of Materials Chemistry C, 2015, 3, 12230-12235.	2.7	21
59	Tunable ferromagnetic ordering in MoS ₂ nanosheets with fluorine adsorption. Nanoscale, 2015, 7, 4211-4216.	2.8	65
60	Hierarchical ultrathin Mo(S _x Se _{1â^'x}) ₂ nanosheets with tunable ferromagnetism and efficient hydrogen evolution reaction activity: towards defect site effect. CrystEngComm, 2015, 17, 6420-6425.	1.3	23
61	Unexpected surface superparamagnetism in antiferromagnetic Cr ₂ O ₃ nanoparticles. RSC Advances, 2015, 5, 46705-46710.	1.7	8
62	Enhanced hydrogen evolution catalysis in MoS ₂ nanosheets by incorporation of a metal phase. Journal of Materials Chemistry A, 2015, 3, 24414-24421.	5.2	88
63	Abnormal room temperature ferromagnetism in CuO–ZnO heterostructures: interface related or not?. Chemical Communications, 2015, 51, 1151-1153.	2.2	16
64	Realization of high Curie temperature ferromagnetism in atomically thin MoS ₂ and WS ₂ nanosheets with uniform and flower-like morphology. Nanoscale, 2015, 7, 650-658.	2.8	94
65	Ferromagnetism in ultrathin MoS2 nanosheets: from amorphous to crystalline. Nanoscale Research Letters, 2014, 9, 586.	3.1	63
66	Observation of room temperature ferromagnetism in pure La2O3 nanoparticles. Applied Physics A: Materials Science and Processing, 2014, 116, 1293-1298.	1.1	15
67	Room temperature ferromagnetism in CuO/Cu2O microspheres: Towards interface effect. Applied Physics Letters, 2014, 104, .	1.5	31
68	Solvothermal synthesis of magnetic copper nitride nanocubes with highly electrocatalytic reduction properties. RSC Advances, 2014, 4, 14206-14209.	1.7	30
69	Porous tin disulfide nanosheets with room temperature ferromagnetic nature. CrystEngComm, 2014, 16, 7876.	1.3	23
70	A series of unexpected ferromagnetic behaviors based on the surface-vacancy state: an insight into NiO nanoparticles with a core–shell structure. RSC Advances, 2014, 4, 46133-46140.	1.7	34
71	Defect-related ferromagnetism in ultrathin metal-free g-C3N4 nanosheets. Nanoscale, 2014, 6, 2577.	2.8	167
72	Singly-charged oxygen vacancy-induced ferromagnetism in mechanically milled SnO ₂ powders. RSC Advances, 2014, 4, 45467-45472.	1.7	57

BAORUI XIA

#	Article	IF	CITATIONS
73	Intrinsic ferromagnetism in hexagonal boron nitride nanosheets. Journal of Chemical Physics, 2014, 140, 204701.	1.2	24
74	Hydrothermal epitaxy and resultant properties of EuTiO3 films on SrTiO3(001) substrate. Nanoscale Research Letters, 2014, 9, 266.	3.1	9
75	Ferromagnetism in ultrathin VS2 nanosheets. Journal of Materials Chemistry C, 2013, 1, 5909.	2.7	149
76	Ferromagnetism in exfoliated tungsten disulfide nanosheets. Nanoscale Research Letters, 2013, 8, 430.	3.1	97
77	Origin of the unexpected room temperature ferromagnetism: formation of artificial defects on the surface in NaCl particles. Journal of Materials Chemistry C, 2013, 1, 6216.	2.7	13
78	Synthesis and characterization of shape-controlled mesoporous Co ₃ O ₄ hierarchical nanostructures. RSC Advances, 2013, 3, 508-512.	1.7	14
79	Ferromagnetism in freestanding MoS2 nanosheets. Nanoscale Research Letters, 2013, 8, 129.	3.1	180
80	Interface mediated ferromagnetism in bulk CuO/Cu2O composites. Applied Physics Letters, 2012, 101, .	1.5	23
81	One-step synthesis of open-cell Ni foams by annealing the Ni2+-based precursor in air. Journal of Materials Chemistry, 2012, 22, 9462.	6.7	10
82	Synthesis and magnetic properties of CuFe2O4 nanotube arrays. Journal Wuhan University of Technology, Materials Science Edition, 2012, 27, 550-554.	0.4	3
83	<i>d</i> ferromagnetism in undoped sphalerite ZnS nanoparticles. Applied Physics Letters, 2011, 99, .	1.5	71
84	Transforming from paramagnetism to room temperature ferromagnetism in CuO by ball milling. AIP Advances, 2011, 1, .	0.6	19
85	Effect of annealing temperature on the magnetic properties of Zn _{0.97} Al _{0.03} O nanoparticles. Physica Status Solidi (A) Applications and Materials Science, 2011, 208, 2454-2459.	0.8	2
86	Magnetic properties of Er-doped ZnO films prepared by reactive magnetron sputtering. Applied Physics A: Materials Science and Processing, 2010, 100, 79-82.	1.1	37
87	Vacancy-Mediated Magnetism in Pure Copper Oxide Nanoparticles. Nanoscale Research Letters, 2010, 5, 769-772.	3.1	171
88	Synthesis, Magnetic Anisotropy and Optical Properties of Preferred Oriented Zinc Ferrite Nanowire Arrays. Nanoscale Research Letters, 2010, 5, 1289-1294.	3.1	87
89	Room-Temperature Ferromagnetism of Flowerlike CuO Nanostructures. Journal of Physical Chemistry C, 2010, 114, 18347-18351.	1.5	163
90	Room temperature ferromagnetism of Cu doped ZnO nanowire arrays. Journal of Applied Physics, 2009, 105, .	1.1	34

	BAOI	BAORUI XIA		
#	Article	IF	CITATIONS	
91	Room temperature ferromagnetism of pure ZnO nanoparticles. Journal of Applied Physics, 2009, 105, .	1.1	178	